analytical chemistry

Open Access

This article is licensed under CC-BY 4.0

pubs.acs.org/ac

Technical Note

# Quasi-Simultaneous Detection of Ammonia and Nitrous Oxide by Photoacoustic Phase-Resolved Method: A Proof-of-Concept

Daniel da Silva Santos, Leonardo Mota, Guilherme Rodrigues Lima, Eduardo César da Matta, Thiago Lemos Alvarenga, Marc-Simon Bahr, Israel Andrade Esquef, Marcus Wolff, and Marcelo Gomes da Silva*

Cite This: https://doi.org/10.1021/acs.analchem.5c04976

Read Online

ACCESS | Metrics & More | Article Recommendations

**ABSTRACT:** This work presents a method for the quasi-simultaneous detection of trace gas molecules using photoacoustic spectroscopy with phase-resolved method. By utilizing two lasers to excite ammonia ($NH_3$) and nitrous oxide ($N_2O$) in a mixture and employing phase-sensitive detection, the individual contributions of these gases were separated. The separation was achieved by adjusting the phase modulation of the $N_2O$ exciting laser until a 90-degree phase difference was established between its signal and that of $NH_3$. The results demonstrate the absence of spectral overlap between the two compounds, enabling independent and quasi-simultaneous detection. Calibration curves highlighted the behavior and cross-interference between $NH_3$ and $N_2O$. For $NH_3$, linear profiles with regression coefficients $R$ = 0.998 and $R$ = 0.999 were observed, when $N_2$ or $N_2$ + $N_2O$ were used as diluent gases, respectively. The corresponding sensitivities were (3.0 ± 0.1) $\mu$V·ppmv$^{-1}$and (3.10 ± 0.08) $\mu$V·ppmv$^{-1}$. The lower detection limits (LDLs) were 51 ppbv and 67 ppbv, respectively. For $N_2O$, calibration data were similarly robust with LDLs of 262 ppbv and 255 ppbv when diluted with $N_2$ and $N_2$ + $NH_3$, respectively. Minimal cross-interference effects were found, confirming the selectivity and reliability of this method for quantifying $NH_3$ and $N_2O$ in gas mixtures. The technique offers advantages over other methods and is applicable to studying emissions related to agriculture with nitrogen fertilizers.

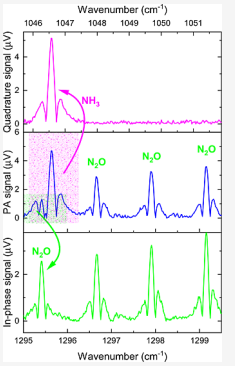


## INTRODUCTION

Spectroscopic techniques have been successfully employed for gas detection in the near- and mid-infrared regions paired with solid-state radiation sources such as quantum cascade lasers (QCLs),[1] interband cascade lasers (ICLs),[2] laser-diode-pumped crystals,[3] and optical parametric oscillator.[4] Among these techniques, photoacoustic spectroscopy (PAS) is particularly notable for trace-level gas sensing because of its high sensitivity, selectivity, and real-time measurement capability. Progress includes the development of new devices equipped with sensitive microphones,[5] cantilever-enhanced,[6] or quartz-enhanced PAS (QEPAS).[7−10] Besides, the fabrication of cost-effective PA cells achieved through 3D printing technologies has appeared.[11]

Simultaneous detection of multiple gases is of paramount importance in environmental monitoring, industrial safety, and medical diagnostics, where rapid and precise multicomponent analysis enables real-time decision-making and improves process efficiency. For instance, QCL-based dual-spectroscopy systems have enabled simultaneous monitoring of CO, $N_2O$, and $H_2O$ with high spectral resolution and rapid acquisition rates.[12] Self-calibrated 2$f$/1$f$ wavelength modulation spectroscopy techniques achieve inherent calibration and stability, minimizing errors associated with laser intensity fluctuations.[13] Furthermore, quartz crystal tuning fork-enhanced laser spectroscopy has shown noteworthy performance for simultaneous detection of three species (e.g., $H_2O$, $CO_2$, and $CH_4$) with ppmv sensitivity and compact configuration.[14]

Recent advancements in PAS research have focused on the "simultaneous detection" of multiple molecules, with frequency division multiplexing (FDM) and time division multiplexing (TDM) emerging as the most widely used methods. Nevertheless, while TDM requires modulation at different frequencies in a temporal sequence or alternation between radiation sources, FDM signals may experience greater attenuation, leading to uneven sensitivity, which could be problematic.[15−21] Yet, there is a lack of literature that addresses the temporal resolution of "simultaneous" measurements in a single resonator.[22,23] This highlights the complexity of utilizing multiple laser sources operating at the same resonance frequency within a straightforward experimental setup.

A related technique, phase-resolved method (PRM) relies on the assumption that distinct absorbing centers are present,

Received: August 13, 2025
Revised: November 17, 2025
Accepted: November 18, 2025

Downloaded via 187.62.131.81 on December 10, 2025 at 21:44:43 (UTC).
See https://pubs.acs.org/sharingguidelines for options on how to legitimately share published articles.

ACS Publications

© XXXX The Authors. Published by American Chemical Society

which inherently entails a phase difference between them due to different nonradiative and thermal relaxation times ($\tau$ and $\tau_\beta$). This approach has been shown to work effectively for solid, liquid and biological samples.[24−28] However, a central challenge in PA-based simultaneous gas detection still remains: extracting overlapping signals when molecular relaxation times are nearly identical.

The very first use of phase-sensitive detection to distinguish gas molecules in multicomponent mixtures was reported by Kosterev et al., in 2004.[29] They employed a QEPAS-based system operating at about $f$ = 32.7 kHz, a reduced pressure (50 Torr) and a second-harmonic wavelength-modulated (WM-2$f$) QCL as a radiation source − such conditions ensure high sensitivity for QEPAS. Moreover, since $\tau$ is longer at lower pressures, the authors stated that an observable phase is detected when the condition $2\pi f \geq \tau^{-1}$ is fulfilled. Hence, they applied PRM to detect carbon monoxide merged in propene. To the best of our knowledge, though under very specific circumstances, this study remains the sole instance to date that addresses the application of PRM in gaseous molecules. The breakthrough of our work consists of electronically phase-shifting the QCLs' wave modulation to introduce a controlled (measurable) phase lag between the generated PA signals. This framework allowed us to completely separate the absorption spectra of $NH_3$ and $N_2O$ from a single quasi-simultaneous measurement of a gas mixture.

**Theoretical Aspects of Phase-Resolved Method.** For a simplified approach, when heat diffusion and dynamic viscosity are neglected, Morse and Ingard derived the inhomogeneous wave equation that relates the acoustic pressure $p$ and the heat source $H$[30]

$$\nabla^2 p - \frac{1}{c^2}\frac{\partial^2 p}{\partial t^2} = -\frac{\gamma - 1}{c^2}\frac{\partial H}{\partial t} \tag{1}$$

where $c$ is the sound speed and $\gamma$ is the ratio of specific heats of the gas for constant pressure and volume. Equation 1 is solved by considering the periodic heating ($\omega$) induced by photon absorption in the gas species, and can be expressed as a superposition of normal acoustic modes $p_k(r,\omega)$. The solution to eq 1 for the case of cylindrical geometry is provided elsewhere.[31,32]

All measurements reported in this work were conducted using the first longitudinal resonance mode of the photoacoustic cell ($k$ = 1). Under this condition, the photoacoustic signal can be expressed by eq 2

$$S(\tilde{\nu}) = p_1(r_{\text{mic}},\omega_1)R_{\text{mic}} = C_{\text{cell}}\cdot P(\tilde{\nu})\cdot N\cdot\sigma(\tilde{\nu}) \tag{2}$$

where $R_{\text{mic}}$ is the microphone sensitivity given in millivolts per pascal; $P(\tilde{\nu})$ is the laser power at $\tilde{\nu}$; $N$ is the density of the absorbing molecules; $\sigma(\tilde{\nu})$ is their absorption cross-section at $\tilde{\nu}$; and $C_{\text{cell}}$ denotes the cell constant, which depends on both the microphone sensitivity and the geometrical configuration of the cell.[31]

When the laser radiation at wavenumber $\tilde{\nu}_0$ passes through the absorbing medium, a fraction of the optical power is converted into heat through nonradiative relaxation processes. The absorbed power per unit volume, $H$, is therefore proportional to the number density of absorbing molecules $N$, the absorption cross section $\sigma(\tilde{\nu}_0)$, and the laser power $P(\tilde{\nu}_0)$ at the corresponding wavenumber. By varying the laser temperature to tune the central wavenumber $\tilde{\nu}_0$, the molecular absorption spectrum is obtained.

In wavelength modulation spectroscopy, the oscillation of the emission wavenumber around its central value $\tilde{\nu}_0$ is responsible for generating the photoacoustic signal. Then, for small amplitude oscillations of $\tilde{\nu}_0$, $\delta\tilde{\nu} = \frac{\partial\tilde{\nu}}{\partial i}\Big|_{\tilde{\nu}_0}\delta i = \frac{\partial\tilde{\nu}}{\partial i}\Big|_{\tilde{\nu}_0}\delta i_0 \exp[j(\omega t + \phi)]$ where $\delta i_0$ is the amplitude of the laser current modulation, and $\omega$ denotes the angular modulation frequency ($2\pi f$). Under this assumption, the absorption cross section can be expanded in a Taylor series (eq 3)

$$\sigma(\tilde{\nu}) = \sigma(\tilde{\nu}_0) + \frac{\partial\sigma}{\partial\tilde{\nu}}\Big|_{\tilde{\nu}_0}\delta_{\tilde{\nu}_0}(i)e^{j(\omega t+\phi)} + \frac{1}{2}\frac{\partial^2\sigma}{\partial\tilde{\nu}^2}\Big|_{\tilde{\nu}_0}\delta^2_{\tilde{\nu}_0}(i)\, e^{2j(\omega t+\phi)} + \cdots \tag{3}$$

where $\frac{\partial\tilde{\nu}}{\partial i}\Big|_{\tilde{\nu}_0}\delta i_0 = \delta_{\tilde{\nu}_0}$.

Since the second harmonic of the wavelength modulation was utilized (third term of eq 3), the laser was modulated at $\omega_1/2$, and the lock-in detection was performed at $2\omega_1$, thereby enabling the measurement of a derivative photoacoustic signal at the resonance frequency of the photoacoustic cell.

For a sample containing two types of target molecules excited with their respective appropriate radiation sources, the total photoacoustic signal can be expressed by eq 4 below, derived from eqs 2 and 3:

$$\begin{aligned} S_{\tilde{\nu}_0}(t) &= S_{\tilde{\nu}_0,N_2O}(t) + S_{\tilde{\nu}_0,NH_3}(t) \\ S_{\tilde{\nu}_0}(t) &= C_{\text{cell}}[N_{N_2O}P_{N_2O}(\tilde{\nu}_{0,N_2O})\sigma_{N_2O}(\tilde{\nu}_{0,N_2O}) \\ &+ N_{NH_3}P_{NH_3}(\tilde{\nu}_{0,NH_3})\sigma_{NH_3}(\tilde{\nu}_{0,NH_3})] = \frac{C_{cell}}{2} \\ &\left(N_{N_2O}P_{N_2O}(\tilde{\nu}_{0,N_2O})\frac{\partial^2\sigma}{\partial\tilde{\nu}^2}\Big|_{\tilde{\nu}_{0,N_2O}}\delta^2_{\tilde{\nu}_{0,N_2O}}e^{2j(\omega_1 t+\phi_{N_2O})}\right. \\ &\left. + N_{NH_3}P_{NH_3}(\tilde{\nu}_{0,NH_3})\frac{\partial^2\sigma}{\partial\tilde{\nu}^2}\Big|_{\tilde{\nu}_{0NH_3}}\delta^2_{\tilde{\nu}_{0NH_3}}e^{2j(\omega_1 t+\phi_{NH_3})}\right) \end{aligned} \tag{4}$$

where $\phi_{N_2O}$ and $\phi_{NH_3}$ are the phases of the photoacoustic signals of these molecules relative to the excitation source.

When two absorbing centers exhibit similar phases, the direct application of PRM becomes challenging. However, an artificial phase difference ($\Delta\phi = \theta_{FG} \neq 0$) can be introduced by adding a phase shift to the modulation of one of the radiation sources (eq 5):

$$S_{\tilde{\nu}_0}(t) = S_{\tilde{\nu}_0,N_2O}e^{2j(\omega_1 t+\phi_{N_2O}+\theta_{FG})} + S_{\tilde{\nu}_0,NH_3}e^{2j(\omega_1 t+\phi_{NH_3})} \tag{5}$$

here, $S_{\tilde{\nu}_{0,m}} = \frac{C_{\text{cell}}}{2}N_m P_m(\tilde{\nu}_{0,m})\frac{\partial^2\sigma}{\partial\tilde{\nu}^2}\Big|_{\tilde{\nu}_{0,m}}\delta^2_{\tilde{\nu}_{0,m}}$, where the subscript $m$ refers to the target gas, which can be either $N_2O$ or $NH_3$, represents the amplitudes of the $N_2O$ and $NH_3$ signals; and $\theta_{FG}$ is the phase increment applied to the $N_2O$ excitation, set using a function generator.

**Experimental Details.** The PA experimental arrangement is depicted in Figure 1. This setup includes two radiation sources: one for detecting $NH_3$ within the spectral range from 1045.70 to 1051.88 $cm^{-1}$ (Thorlabs, ICL-QD9556HHLH-A) and another for detecting $N_2O$ in the spectral range from


https://doi.org/10.1021/acs.analchem.5c04976
Anal. Chem. XXXX, XXX, XXX−XXX

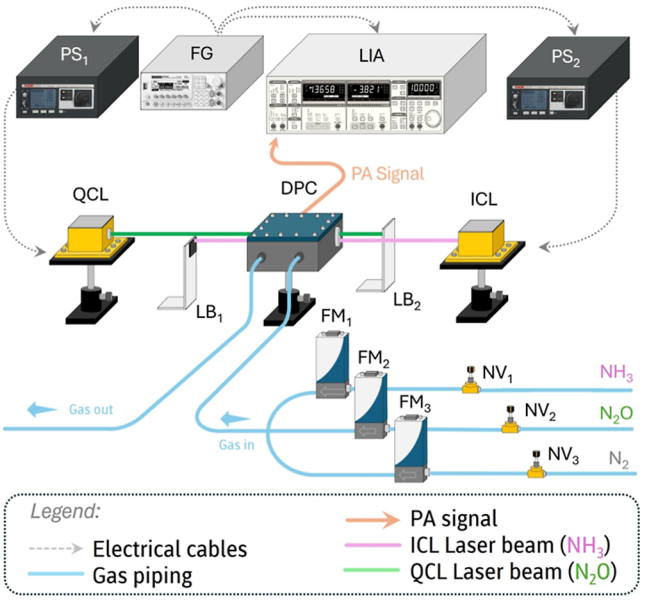


**Figure 1.** Experimental apparatus dedicated to quasi-simultaneous measurements of $NH_3$ and $N_2O$. The acronyms are defined as PS (Power Supply), FG (Function Generator), LIA (Lock-In Amplifier), DPC (Differential Photoacoustic Cell), LB (Laser Block), FM (Flow Meter) and NV (Needle Valve).

1295.00 to 1299.50 $cm^{-1}$ (Thorlabs, QCL-QD7716HH). The wavenumber scan was obtained by varying the temperature of $N_2O$ laser holder between 15 °C (53 mW) and 45 °C (34.4 mW) and that of $NH_3$ laser holder between 20 °C (88.0 mW) and 50 °C (67.0 mW), at a temperature rate of 0.05 $°Cs^{-1}$. The wavenumber-to-temperature tuning rates were 0.150 $cm^{-1}/°C$ and 0.206 $cm^{-1}/°C$ for $N_2O$ and $NH_3$, respectively. To prevent laser damage due to cross-interference, each beam was slightly tilted and blocked to avoid entering the opposite laser. Two power supplies (Thorlabs, ITC4002QCL) individually powered the lasers.

The gas sensor consists of a differential photoacoustic cell (DPC) with the first longitudinal (out-of-phase ring resonance[11]) mode at 3.9 kHz and a quality factor of about 15. It is equipped with two microphones to detect the photoacoustic signal.[11] The microphone signals are amplified using a digital lock-in amplifier (Stanford Research SR830), set to a time constant of 0.3 s and employing a second-order low-pass filter (12 dB roll-off). A sampling rate of 0.5 Hz was established in the Python-written data acquisition program.

Second-harmonic wavelength modulation (WM-2f) was achieved by superimposing a sinusoidal AC current with a peak-to-peak amplitude of 8 mA on a DC bias current of 295 mA for $N_2O$ and on a DC bias current of 520 mA for $NH_3$. A function generator with two synchronized output channels (RIGOL DG 1022) was employed.

The AC frequency was adjusted to be half of the DPC's resonance frequency ($f/2$), and the lock-in amplifier was configured to measure the second harmonic ($f$).[33] The output channel of the function generator used for the modulation of $N_2O$ allows phase increments relative to that of the other channel, enabling the temporal separation of the photoacoustic signals from both molecules on a measurable scale. The photoacoustic signal $S$ as a function of time is given by eq 5.

Starting from certified standard samples of 5.0 ppmv of $N_2O$ in nitrogen and 10 ppmv of $NH_3$ in nitrogen, both supplied by White Martins Ltd., different diluted concentrations of the two species were prepared by mixing them with each other or with pure nitrogen (99.9%). The dilution ratios were manually adjusted using mechanical valves and monitored with mass flow meters (Alicat Scientific, M-500SCCM-D/5M). For all mixtures, the total gas flow rate was maintained at 300 sccm.

## RESULTS AND DISCUSSION

The WM-2f PA spectra of a gas mixture containing 4.67 ppmv $NH_3$ (140 sccm) and 2.67 ppmv $N_2O$ (160 sccm) are shown in Figure 2. The central panel presents the original PA spectrum obtained when both gas species were excited simultaneously. In the first half of the spectrum, an overlap between the absorption lines of $N_2O$ and $NH_3$ occurs. To resolve these features, the PRM technique was applied. Prior to this, since the laser drivers were modulated by a separate output of a dual-channel function generator, a relative time

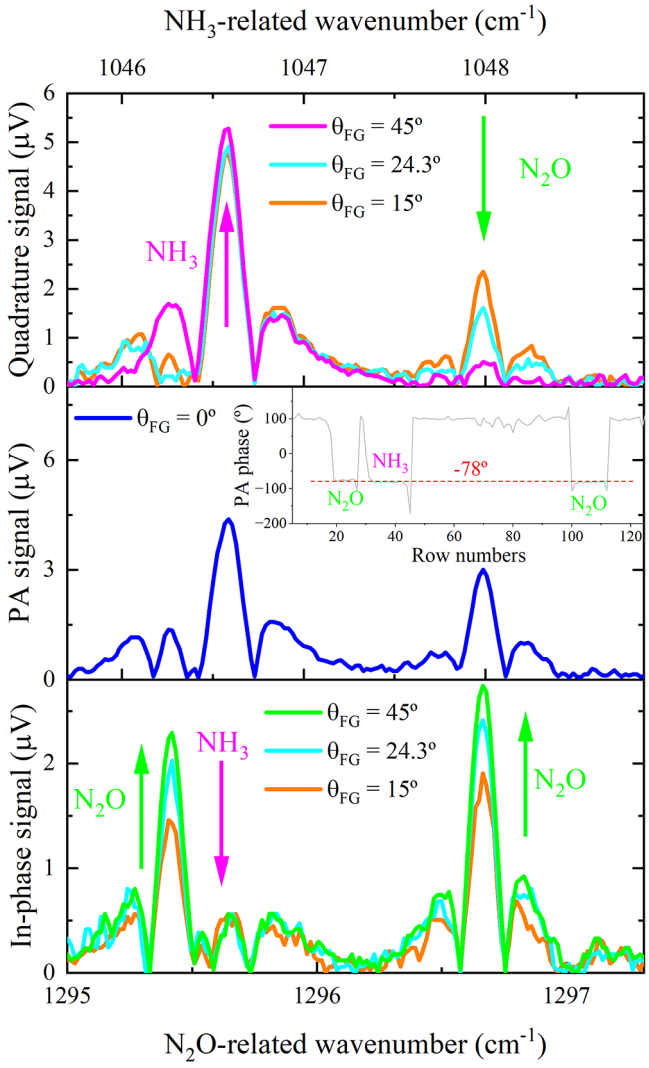


**Figure 2.** WM-2f PA spectra as a function of wavenumber. Central panel is the measured spectrum ($\theta_{FG} = 0°$) of a gas mixture consisting of 4.67 ppmv $NH_3$ and 2.67 ppmv $N_2O$. The upper and bottom panels refer, respectively, to quadrature and in-phase spectra of the same gas mixture for different $\theta_{FG}$ values. The inset figure shows that $2\phi_{N_2O}$ and $2\phi_{NH_3}$ (in eq 5) are nearly identical, both are approximately −78°.


https://doi.org/10.1021/acs.analchem.5c04976
Anal. Chem. XXXX, XXX, XXX−XXX

shift between the $N_2O$ and $NH_3$ laser current modulations was established by setting the phase difference between the channels to $\theta_{FG}$ = 15°, 24.3°, and 45°. In this configuration, a phase shift $\theta_{FG}$ corresponds to a time delay of $\theta_{FG}/360° \times (2/3.9\ kHz)$, where 3.9 kHz represents the resonance frequency of the photoacoustic cell. In other words, a phase shift of $\theta_{FG}$ = 15° corresponds to 15°/360° × (2/3.9 kHz) = 21.4 $\mu$s; $\theta_{FG}$ = 24.3° corresponds to 34.6 $\mu$s; $\theta_{FG}$ = 45° corresponds to 64.1 $\mu$s.

The upper and lower panels depict the quadrature and in-phase PA signals as functions of $\theta_{FG}$, indicating that an increase in $\theta_{FG}$ results in an improved spectral resolution. For $\theta_{FG}$ = 45°, the projection of the $NH_3$ signal is predominantly aligned with the lock-in *Y*-axis (top panel, magenta line). In contrast, the signal derived from $N_2O$ remained nearly constant along the lock-in *X*-axis (bottom panel, green line). Nonetheless, cross-talk between $N_2O$ and $NH_3$ persists, as indicated by a green arrow in the top graph and a magenta arrow in the bottom graph.

Starting from a common natural photoacoustic phase shift of (−78 ± 6)°, this effect is illustrated in Figure 3a–d, wherein

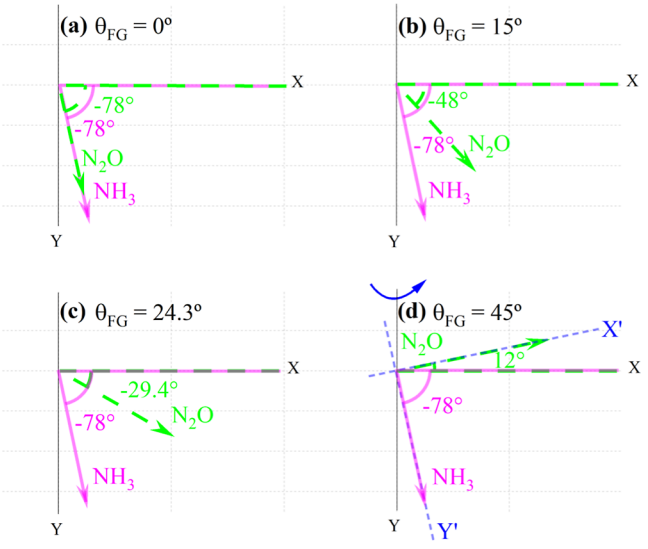


**Figure 3.** Phasor diagram of the PA signal for $NH_3$ and $N_2O$ (dashed green line) as a function of $\theta_{FG}$. From (a to d), $\theta_{FG}$ were set to be 0°, 15°, 24.3° and 45°, respectively. In (d), the short-dashed blue line illustrates the rotation of the reference frame, enabling full isolation of the PA spectra of $NH_3$ along the *Y*′-axis and $N_2O$ along the *X*′-axis.

for each adjusted value of $\theta_{FG}$ on the function generator, the induced phase lag between the PA phasors of $NH_3$ (solid magenta arrow) and $N_2O$ (dashed green arrow) was twice as large (eq 5). Thus, PRM was applied. To do so, the starting point was that when $\theta_{FG}$ = 45°, which implied an effective separation equal to 90°.

Figure 4 portrays the resulting quasi-simultaneous detection of 4.67 ppmv $NH_3$ and 2.67 ppmv $N_2O$. The shaded areas in the middle panel highlight the region where a molecular superposition is clearly observed. From a phasor perspective, it corresponds to the scenario presented in Figure 3a. To achieve complete spectral resolution between $NH_3$ and $N_2O$, the initial configuration was as outlined in Figure 3d, i.e., $\theta_{FG}$ = 45°. From this, progressive rotations of the lock-in reference frame (denoted by the rounded blue arrow) were performed to ascertain a novel arrangement that would allow complete

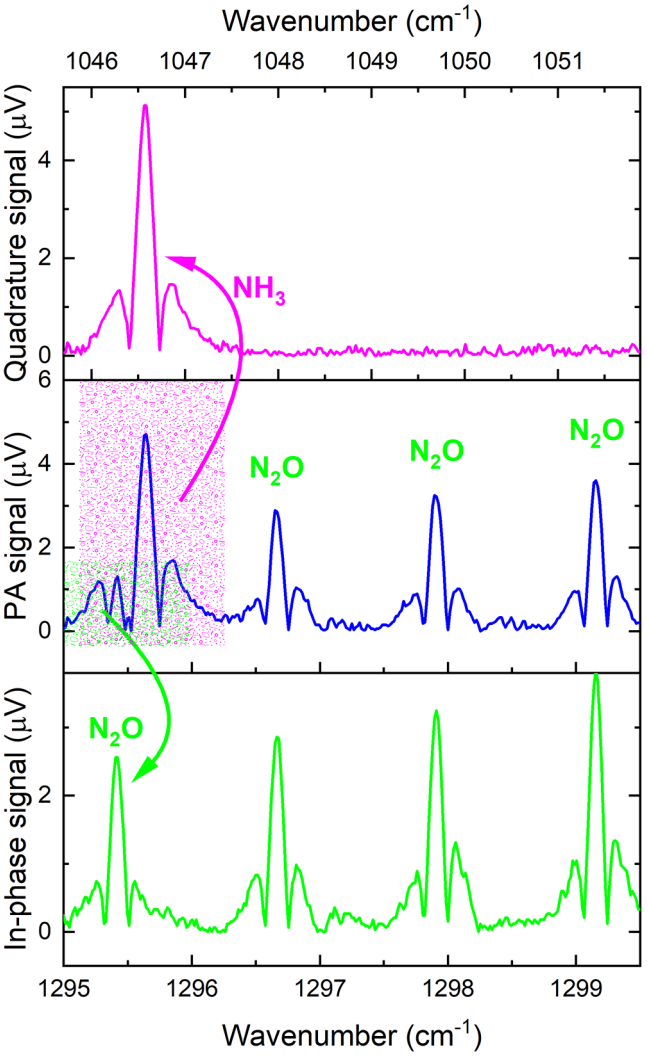


**Figure 4.** Resulting PA–PRM for $NH_3$ and $N_2O$. The center panel shows the as measured PA spectrum of a mixture containing 4.67 ppmv $NH_3$ plus 2.67 ppmv $N_2O$. The highlighted areas in magenta and green display overlapped lines of $NH_3$ and $N_2O$. The upper and bottom panels correspond, respectively, to the quasi-simultaneously measured quadrature and in-phase spectra taking into account a $\theta_{FG}$ = 45° combined with a 12° lock-in phase increment (rotation of the reference frame).

separation of the PA spectra of $NH_3$ and $N_2O$. This condition was successfully realized when the reference frame was rotated by 12° (short-dashed blue line). As a result, the WM-2f PA spectrum of $NH_3$ was entirely phase-resolved in the quadrature component (upper panel of Figure 4), while the in-phase component unequivocally exhibited the characteristic WM-2f PA spectrum of $N_2O$ (bottom panel of Figure 4).

**Calibration Curves: Phase Behavior, Sensitivity, Detection Limit and Cross-Talk between $NH_3$ and $N_2O$.** Figure 5 displays the PA phases as functions of $N_2O$ and $NH_3$ concentrations. Each data point represents the average of 300 measurements (inset plot in Figure 5), and the error bar corresponds to their standard deviation. The PRM was applied by initially setting the signal phase to −90° when only 2.0 ppmv of $NH_3$, diluted in nitrogen and free from $N_2O$, was flowing through the PA cell. The same approach was applied for 4.0 ppmv $N_2O$ in nitrogen, free from $NH_3$, with its phase set to 0°. Subsequently, in separate experiments, further


https://doi.org/10.1021/acs.analchem.5c04976
Anal. Chem. XXXX, XXX, XXX−XXX

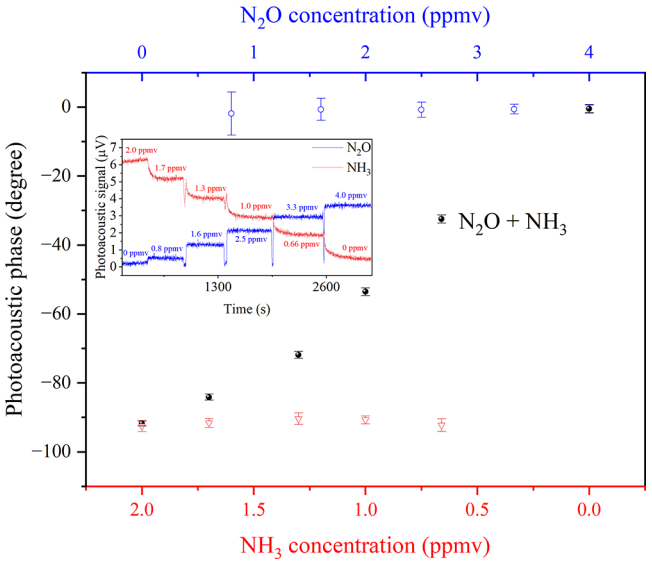


**Figure 5.** Photoacoustic phase response as a function of gas concentration measured by the PRM. The top horizontal axis shows the concentration of $N_2O$ in $N_2$, while the bottom horizontal axis shows the concentration of $NH_3$ in $N_2$. The vertical axis represents the photoacoustic phase. Blue symbols correspond to the phase of $N_2O$ measured separately at different concentrations in $N_2$. Red symbols represent the phase of $NH_3$ measured separately at different concentrations in $N_2$. Black symbols indicate the phase of the gas mixture during simultaneous dilution of $NH_3$ and $N_2O$ in $N_2$. The inset displays the quadrature signal of $NH_3$ (red) and the in-phase signal of $N_2O$ (blue) in the PRM measurement of the mixture, illustrating the phase differentiation between the two gases.

dilutions of both gases in nitrogen were prepared, and the signal phases for each molecule at four new concentrations were measured (open blue circles for $N_2O$ and red triangles for $NH_3$, Figure 5). In a second experiment, involving mixtures of $NH_3$, $N_2O$, and $N_2$, the gas components were combined in flow to reproduce the same concentrations of $N_2O$ and $NH_3$ as in the previous experiment. The phase values of the signal for each gas mixture are plotted as black filled circles in Figure 5. Consequently, the PA signal phase varies according to the relative contributions of both molecular species. This trend is illustrated by the black points in Figure 5, where the PA phase approaches 0° as the $N_2O$ concentration increases to 4 ppmv in the absence of $NH_3$, and approaches −90° when the $NH_3$ concentration reaches 2 ppmv in the absence of $N_2O$. These results strongly support the effectiveness of phase separation and gaseous detection across different concentrations using the proposed approach.

With the aim of investigating both the PRM performance and the occurrence of cross-talk between $N_2O$ and $NH_3$, Figure 6 depicts the calibration curves (open symbols), while the solid lines represent the best linear fits to the experimental data. In Figure 6a, the quadrature signals from $NH_3/N_2$ (orange circles) and $NH_3/N_2 + N_2O$ (blue circles) can be seen. From the fitting parameters, fairly good linear trends ($R_{NH_3/N_2} = 0.998$ and $R_{NH_3/N_2+N_2O} = 0.999$) of the PA signal as a function of the concentration between 0 and 2.0 ppmv were obtained. Besides, the sensitivities (slopes of linear fits) were calculated as $\text{slope}_{(NH_3/N_2)} = (3.0 \pm 0.1)\ \mu V \cdot ppmv^{-1}$ and $\text{slope}_{(NH_3/N_2+N_2O)} = (3.10 \pm 0.08)\ \mu V \cdot ppmv^{-1}$. These latter information in conjunction with the standard deviation of the

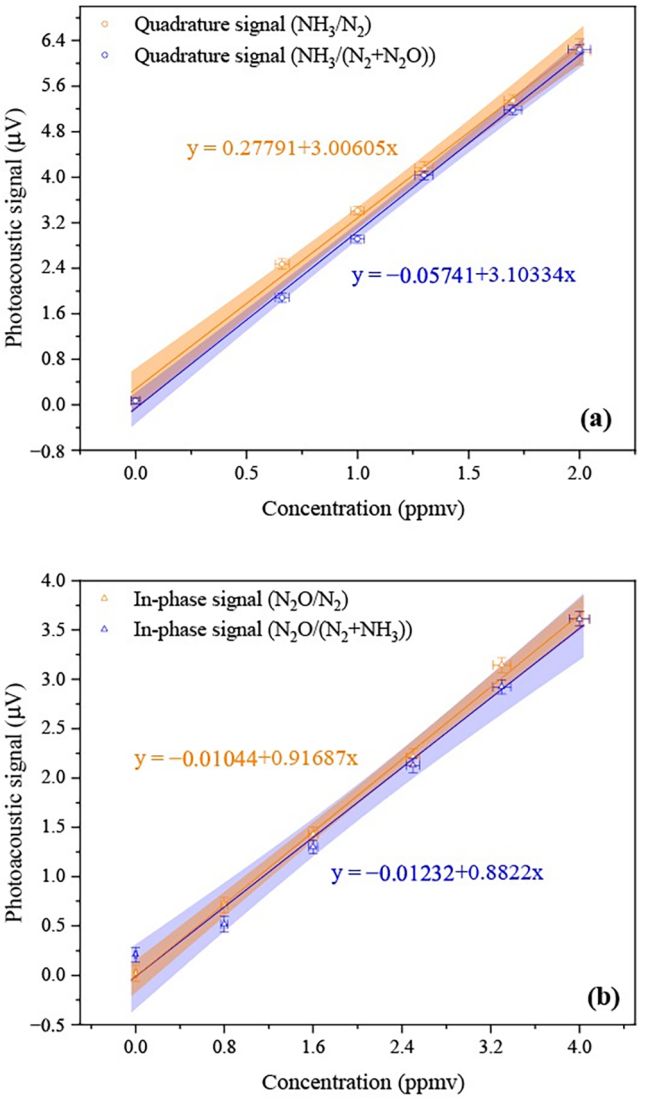


**Figure 6.** Calibration curves for photoacoustic measurements of $NH_3$ (a) and $N_2O$ (b). Experimental points are shown with horizontal and vertical error bars representing the standard deviations of the gas concentration and photoacoustic signal, respectively. Solid lines denote the best linear fits, and shaded regions indicate the 95% confidence bands of the regression.

background multiplied by three ($3\sigma_{Bg}$) − here regarded as the minimal detection threshold − can be utilized to deduce the system lower detection limit (LDL), similarly as did by a contemporary research.[34] By considering $\sigma_{Bg(NH_3/N_2)} = 52$ nV and $\sigma_{Bg(NH_3/N_2+N_2O)} = 67$ nV the corresponding LDLs of 51 and 67 ppbv were estimated.

In Figure 6b, the in-phase amplitude measurements for $N_2O/N_2$ (represented by orange triangles) and $N_2O/N_2 + NH_3$ (designated by blue triangles) are illustrated. The data yielded fitting curves that also exhibited strong linear correlations ($R_{N_2O/N_2} = 0.999$ and $R_{N_2O/N_2+NH_3} = 0.994$) of the PA magnitude as a function of concentration within the range of 0−4.0 ppmv. Sensitivity analyzes, analogous to those performed for $NH_3$, resulted in sensitivity values of $\text{slope}_{(N_2O/N_2)} = (0.92 \pm 0.02)\ \mu V \cdot ppmv^{-1}$ and $\text{slope}_{(N_2O/N_2 + NH_3)} = (0.88 \pm 0.05)\ \mu V \cdot ppmv^{-1}$. Taking into account the standard deviations $\sigma_{Bg(N_2O/N_2)} = 80$ nV and $\sigma_{Bg(N_2O/N_2 + NH_3)} =$


https://doi.org/10.1021/acs.analchem.5c04976
Anal. Chem. XXXX, XXX, XXX−XXX

75 nV, the LDLs were calculated to be 262 and 255 ppbv, respectively.

Each calibration point in Figure 6 is presented with both horizontal and vertical error bars, representing the standard deviations of the gas concentration and the photoacoustic signal, respectively. Additionally, the shaded regions surrounding the fitted lines indicate the 95% confidence intervals for linear regression, visually expressing the statistical reliability of the calibration and regression parameters throughout the examined concentration range.

A comparative analysis of the sensitivities provides insight not only into LDLs but also on potential cross-interference effects between $NH_3$ and $N_2O$. For $NH_3$, the sensitivity coefficients ((3.0 ± 0.1) $\mu V \cdot ppmv^{-1}$and (3.10 ± 0.08) $\mu V \cdot ppmv^{-1}$) showed a slight difference, well within the range of their respective uncertainties. Similarly, for $N_2O$, the sensitivity values displayed ((0.92 ± 0.02) $\mu V \cdot ppmv^{-1}$and (0.88 ± 0.05) $\mu V \cdot ppmv^{-1}$) negligible variation. These results suggest that the presence of either analyte in the gas matrix does not give rise to significant cross-talk or mutual interference under the experimental conditions evaluated. The overall calibration trends are robust, thereby confirming the reliability and selectivity of the PA−PRM for independent quantification of $NH_3$ and $N_2O$.

## CONCLUSIONS AND OUTLOOK

We introduced a new method for the concurrent sensing of trace gas molecules using photoacoustic (PA) spectroscopy. By inducing a phase difference in the modulation, distinct excitation times are created for $NH_3$ and $N_2O$, allowing separate absorption spectra via phase-resolved measurements (PRM). The results show no spectral overlap between $NH_3$ and $N_2O$, enabling independent quasi-simultaneous detection. The calibration curves helped evaluate the behavior and cross-interference between $NH_3$ and $N_2O$. For $NH_3$, linear profiles ($R$ = 0.998 and $R$ = 0.999) were acquired when $N_2$ or $N_2$ + $N_2O$ were adopted as diluting gas. The corresponding sensitivities were (3.0 ± 0.1) $\mu V \cdot ppmv^{-1}$ and (3.10 ± 0.08) $\mu V \cdot ppmv^{-1}$, respectively. Using the criterion of the $3\sigma_{Bg}$ detection threshold ($\sigma_{Bg(NH_3/N_2)}$ = 52 nV and $\sigma_{Bg(NH_3/N_2+N_2O)}$ = 67 nV) the lower detection limits (LDLs) were determined to be 51 and 67 ppbv, respectively. For $N_2O$, measurements yielded equally robust calibration data, with regression coefficients of $R$ = 0.999 ($N_2O/N_2$) and $R$ = 0.994 ($N_2O/N_2$ + $NH_3$). Sensitivity analysis produced values of (0.92 ± 0.02) $\mu V \cdot ppmv^{-1}$and (0.88 ± 0.05) $\mu V \cdot ppmv^{-1}$, with corresponding LDLs of 262 and 255 ppbv based on ($\sigma_{Bg(N_2O/N_2)}$ = 80 nV and $\sigma_{Bg(N_2O/N_2+NH_3)}$ = 75 nV). Comparative analysis of the sensitivities reveals minimal cross-interference effects. For $NH_3$, the sensitivity coefficients differed only within their combined uncertainties, while $N_2O$ sensitivities displayed negligible variation between single-component and binary-mixture scenarios. Error bars representing both gas concentration and PA signal uncertainties, along with 95% confidence intervals for the linear regressions, demonstrate the statistical reliability of the calibration throughout the examined range. These results confirm that the presence of either chemical species does not induce significant cross-talk, thus validating the selectivity and reliability of PRM approach for independent and quasi-simultaneous quantification of $NH_3$ and $N_2O$ in gas mixtures. This technique is relatively easy to implement and offers significant advantages over other methods. It also has potential applications in the study of $NH_3$ and $N_2O$ emissions, especially those related to agriculture involving nitrogen fertilizers.

## AUTHOR INFORMATION


### Corresponding Author

**Marcelo Gomes da Silva** − *Universidade Estadual do Norte Fluminense Darcy Ribeiro, Campos dos Goytacazes 28013-602 Rio de Janeiro, Brazil;* orcid.org/0000-0001-5440-8245; Email: mgs@uenf.br

### Authors

**Daniel da Silva Santos** − *Universidade Estadual do Norte Fluminense Darcy Ribeiro, Campos dos Goytacazes 28013-602 Rio de Janeiro, Brazil;* orcid.org/0009-0003-9463-2307

**Leonardo Mota** − *Universidade Estadual do Norte Fluminense Darcy Ribeiro, Campos dos Goytacazes 28013-602 Rio de Janeiro, Brazil*

**Guilherme Rodrigues Lima** − *Universidade Federal do Espírito Santo, Alto Universitário, Alegre 29500-000 Espírito Santo, Brazil*

**Eduardo César da Matta** − *Universidade Estadual do Norte Fluminense Darcy Ribeiro, Campos dos Goytacazes 28013-602 Rio de Janeiro, Brazil*

**Thiago Lemos Alvarenga** − *Universidade Estadual do Norte Fluminense Darcy Ribeiro, Campos dos Goytacazes 28013-602 Rio de Janeiro, Brazil*

**Marc-Simon Bahr** − *Heinrich Blasius Institute of Physical Technologies, Hamburg University of Applied Sciences, Hamburg 20999, Germany*

**Israel Andrade Esquef** − *Universidade Estadual do Norte Fluminense Darcy Ribeiro, Campos dos Goytacazes 28013-602 Rio de Janeiro, Brazil*

**Marcus Wolff** − *Heinrich Blasius Institute of Physical Technologies, Hamburg University of Applied Sciences, Hamburg 20999, Germany*

Complete contact information is available at: https://pubs.acs.org/10.1021/acs.analchem.5c04976



### Funding

The Article Processing Charge for the publication of this research was funded by the Coordenacao de Aperfeicoamento de Pessoal de Nivel Superior (CAPES), Brazil (ROR identifier: 00x0ma614).

### Notes

The authors declare no competing financial interest.


## ACKNOWLEDGMENTS

This research received financial support from Fundação Carlos Chagas Filho de Amparo à Pesquisa do Estado do Rio de Janeiro (FAPERJ − grant numbers E-26/211.213/2021, E-26/211.398/2021, E-26/211.777/2021), Conselho Nacional de Desenvolvimento Científico e Tecnológico (CNPq − grant number 406271/2021-6). M.W. and M.G.S. are grateful to the Deutscher Akademischer Austauschdienst and Coordenação de Aperfeiçoamento de Pessoal de Nível Superior through the International Cooperation Program "PROBRAL" (DAAD and CAPES − Finance Code 001). D.S.S. and M.-S.B. acknowledge, respectively, CAPES and DAAD for the scholarships provided during their stays at HAW and UENF.



https://doi.org/10.1021/acs.analchem.5c04976
Anal. Chem. XXXX, XXX, XXX−XXX

## REFERENCES


(1) Giglio, M.; Zifarelli, A.; Sampaolo, A.; Menduni, G.; Elefante, A.; Blanchard, R.; Pfluegl, C.; Witinski, M. F.; Vakhshoori, D.; Wu, H.; Passaro, V. M.; Patimisco, P.; Tittel, F. K.; Dong, L.; Spagnolo, V. *Photoacoustics* **2020**, *17*, 100159.
(2) Yang, R. Q.; Santos, M. B. *Photonics* **2025**, *12*, 155.
(3) Qiao, S.; He, Y.; Sun, H.; Patimisco, P.; Sampaolo, A.; Spagnolo, V.; Ma, Y. *Light: Sci. Appl.* **2024**, *13*, 100.
(4) Gomes da Silva, M.; Miklos, A.; Falkenroth, A.; Hess, P. *Appl. Phys. B:Lasers Opt.* **2006**, *82*, 329−336.
(5) Silva, L. G.; Bueno, S. C. E.; da Silva, M. G.; Mota, L.; Sthel, M. S.; de Castro, M. P. P.; Santiago Neto, R. M.; Kuba, V. M. *Lasers Med Sci.* **2022**, *37*, 983−991.
(6) Yin, Y.; Ren, D.; Li, C.; Chen, R.; Shi, J. *Photoacoustics* **2022**, *28*, 100423.
(7) Wang, F.; Cheng, Y.; Xue, Q.; Wang, Q.; Liang, R.; Wu, J.; Sun, J.; Zhu, C.; Li, Q. *Sens. Actuators, A* **2022**, *345*, 113807.
(8) Ma, Y. *Front. Phys.* **2020**, *8*, 268.
(9) Ma, J.; Fan, E.; Liu, H.; Zhang, Y.; Mai, C.; Li, X.; Jin, W.; Guan, B.-O. *Adv. Photonics* **2024**, *6*, 066008.
(10) Ma, Y.; Qiao, S.; Wang, R.; He, Y.; Fang, C.; Liang, T. *Appl. Phys. Rev.* **2024**, *11*, 041412.
(11) Lima, G. R.; Pelais, A.; Neto, A. G.; Coutinho, M. F.; Esquef, I. A.; Batista, A. G. T.; da Silva, M. G.; Sthel, M. S.; de Castro, M. P. P.; Mota, L. *Measurement* **2024**, *229*, 114422.
(12) Li, J.; Deng, H.; Sun, J.; Yu, B.; Fischer, H. *Sens. Actuators, B* **2016**, *231*, 723−732.
(13) Liu, N.; Xu, L.; Zhou, S.; Zhang, L.; Li, J. *ACS Sens.* **2020**, *5*, 3607−3616.
(14) Xu, L.; Zhou, S.; Liu, N.; Zhang, M.; Liang, J.; Li, J. *Anal. Chem.* **2020**, *92*, 14153−14163.
(15) Wang, F.; Wu, J.; Cheng, Y.; Fu, L.; Zhang, J.; Wang, Q. *Opt. Express* **2023**, *31*, 33898−33913.
(16) Rodriguez Gutierrez, G.; Ortiz Perez, A.; Palzer, S. *ACS Sens.* **2023**, *9*, 23−28.
(17) Wei, Y.; Huang, Q.; Li, J. *Sens. Actuators, A* **2023**, *360*, 114542.
(18) Li, C.; Han, X.; Ma, F.; Zhao, X.; Wang, Z.; Qi, H.; Guo, M.; Chen, K. *Sens. Actuators, B* **2024**, *399*, 134801.
(19) Huang, Q.; Wei, Y.; Li, J. *Sens. Actuators, B* **2022**, *369*, 132234.
(20) Zhang, L.; Liu, L.; Zhang, X.; Yin, X.; Huan, H.; Liu, H.; Zhao, X.; Ma, Y.; Shao, X. *Photoacoustics* **2023**, *31*, 100492.
(21) Sun, J.; Liu, B.; Liu, L.; Huan, H.; Zhang, L.; Zhang, X.; Yang, J.; Shao, X. *Microw. Opt. Technol. Lett.* **2024**, *66*, No. e34039.
(22) Jiang, Y.; Zhang, T.; Wang, G.; He, S. *Appl. Sci.* **2021**, *11*, 5224.
(23) Huang, Y.; Zhang, T.; Wang, G.; He, H.; He, S. *Microchem. J.* **2024**, *203*, 110918.
(24) Jaime, J.; Hernández-Wong, J.; Nogal, U.; Rojas, A.; Calderón, A.; Rojas-Trigos, J.; Muñoz, R.; Juárez-Gracia, G.; Mansanares, A.; Marín, E. *Measurement* **2019**, *138*, 143−148.
(25) Olvera Cano, L. I.; Villanueva Lopez, G. C.; Mateos, E. R.; Orea, A. C. *Appl. Spectrosc.* **2021**, *75*, 1465−1474.
(26) Lara-Bernal, A.; Silva, M. G.; Mota, L.; Marín, E.; Cordeiro, T. C.; Silva, E. C.; Viana, D. A.; Vargas, H.; Polidoro, J. C.; Mello-Monte, M. B. *An. Acad. Bras. Ciênc.* **2022**, *94*, No. e20200512.
(27) Lonni, A. A. S. G.; Dahmer, D.; Costa, I. A. P.; DiCiaula, M. C.; Ritter, M. R.; Bruschi, M. L.; Guimarães, F. B.; Bento, A. C.; Rohling, J. H.; Mello, E. V. S. L.; Natali, M. R. M.; Baesso, M. L.; Mello, J. C. P. *Spectrochim. Acta, Part A* **2022**, *275*, 121152.
(28) Rufino da Silva, C. E.; de Oliveira, M. G.; Baesso, M. L.; Agra, K. L.; Suassuna Filho, J.; da Silva Lima, R. J. *Spectrochim. Acta, Part A* **2023**, *298*, 122761.
(29) Kosterev, A. A.; Bakhirkin, Y. A.; Tittel, F. K.; Blaser, S.; Bonetti, Y.; Hvozdara, L. *Appl. Phys. B:Lasers Opt.* **2004**, *78*, 673−676.
(30) Morse, P. M.; Ingard, K. U. *Theoretical Acoustics*; Princeton University Press, 1986.
(31) Sigrist, M. W. *Air Monitoring by Spectroscopic Techniques*; Wiley: New York, 1994; Vol. *127*.
(32) Hess, P. *Photoacoustic Photothermal and Photochemical Processes in Gases*; Springer, 1989; pp 1−13.
(33) Lima, G. R.; Mota, L.; Miklós, A.; Angster, J.; Dubovski, Z.; Silva, M. G.; Sthel, M. S.; Vargas, H. *Appl. Phys. B* **2014**, *117*, 333−341.
(34) Pangerl, J.; Müller, M.; Rück, T.; Weigl, S.; Bierl, R. *Sens. Actuators, B* **2022**, *352*, 130962.



https://doi.org/10.1021/acs.analchem.5c04976
*Anal. Chem.* XXXX, XXX, XXX−XXX